Renewable Energy 226 (2024) 120454

Contents lists available at ScienceDirect

Renewable Energy

journal homepage: www.elsevier.com/locate/renene

Dynamic response of a shallow-draft floating wind turbine concept: Experiments and modelling

Alicia Terrero-Gonzalez [a], Saishuai Dai [b], Richard D. Neilson [a], Jim Papadopoulos [c], Marcin Kapitaniak [a,*]

[a] National Decommissioning Centre, School of Engineering, University of Aberdeen, Newburgh, AB41 6AA, UK
[b] Kelvin Hydrodynamics Laboratory, Department of Naval Architecture, Ocean and Marine Engineering, University of Strathclyde, Glasgow, G20 0TL, UK
[c] T-Omega Wind Ltd, Aberdeen, AB10 6SD, UK

ARTICLE INFO

Keywords:
Floating Offshore Wind Turbine
Dynamics analysis
RAO
Marine Simulator

ABSTRACT

This paper considers the dynamic response of a novel lightweight FOWT concept being developed by T-Omega Wind Ltd, that is able to float over even steep high waves, and be economical in deep water. The study aims to understand the response to waves during marine operations (installation, or maintenance) as part of optimizing its design. For this purpose real-time 6 degrees-of-freedom (6 DOF) simulations are computed for the system under operational and extreme sea wave scenarios in the state-of-the-art Multiphysics Marine Simulator at the National Decommissioning Centre (NDC). RAOs for heave and pitch displacements are evaluated across varying wave heights and periods of excitation to identify system behaviour including resonant frequencies. The model is calibrated by adjusting system damping parameters for each wave frequency to match experimental tests on a 1:60 scaled prototype at the Kelvin Hydrodynamics Laboratory, resulting in an ad hoc damping expression to produce appropriate system dynamic behaviour for "High" and "Low" Sea States. The study concludes by identifying ranges of wave parameters that limit peak motions, proposes analytical expressions for RAO responses and provides damping parameters that validate the Marine Simulator as a suitable tool to predict FOWT dynamic responses with reduced computation time.

1. Introduction

The commitment to achieving net-zero greenhouse gas emissions by 2050 and the growing interest in harnessing offshore wind energy have propelled the development of Floating Offshore Wind Turbines (FOWT). Wind energy in deeper waters is better for energy harvesting, with steadier and higher wind speeds, compared to shallow waters. To date, most current offshore wind turbines are fixed to the seabed, which is unfeasible for water depths over 60 m [1]. FOWT for deeper water are still in the early development stage, resulting in a very small fraction (0.29%) of the global offshore wind capacity with only 188 MW connected to the grid, of which 171 MW are in Norway (values for the end of 2022) [2,3]. Deep waters hold significant untapped power potential, and FOWT offer advantages such as reducing visual impact from the shore in comparison to fixed platforms, higher theoretical wind power potential, and towing procedures for easier maintenance and deployment [4], among others. In line with these advantages, the Global Wind Energy Council (GWEC) predicts a substantial increase in installed FOWT capacity, with a projected 16.5 GW connected to the grid by 2030, primarily from installations along the UK coast [5]. As of the end of 2022, the Levelized Cost of Energy (LCOE) for FOWT was estimated between 129 and 151 USD/MWh [6]. This relatively high cost is mainly attributed to the technology's immaturity and the associated expenses of the platform, mooring, deployment, maintenance and decommissioning [2]. However, due to growth in deployment and maturation of technology, it is expected that the LCOE will decrease to 100 USD/MWh by 2025 with a further drop to 40 USD/MWh by 2050 [2]. This cost reduction will enhance the market competitiveness of FOWT, aligning it with the current onshore wind energy sector [7].

Several authors have reviewed the various floating-turbine concepts and classified the supporting platforms into major categories: *Spar*, *Tension Leg Platforms (TLP)* [8], *Barge* [9] and *Semi-submersible* types as represented in Fig. 1. However, the classification is not restricted to these designs since other concepts are still being proposed and developed. FOWT are intended for water depths over 30 m [10] and comprise a floating structure, the turbine (single or multi-rotor [11]) on its tower, and the mooring lines connected to the seabed by various types of anchors [12]. Major engineering challenges that must be addressed to advance the technology include ensuring turbine system stability under working and survival conditions [1,13] and understanding how the design influences the dynamics of the turbine system

* Corresponding author.
E-mail address: marcin.kapitaniak@abdn.ac.uk (M. Kapitaniak).

https://doi.org/10.1016/j.renene.2024.120454
Received 1 January 2024; Received in revised form 6 March 2024; Accepted 3 April 2024
Available online 5 April 2024

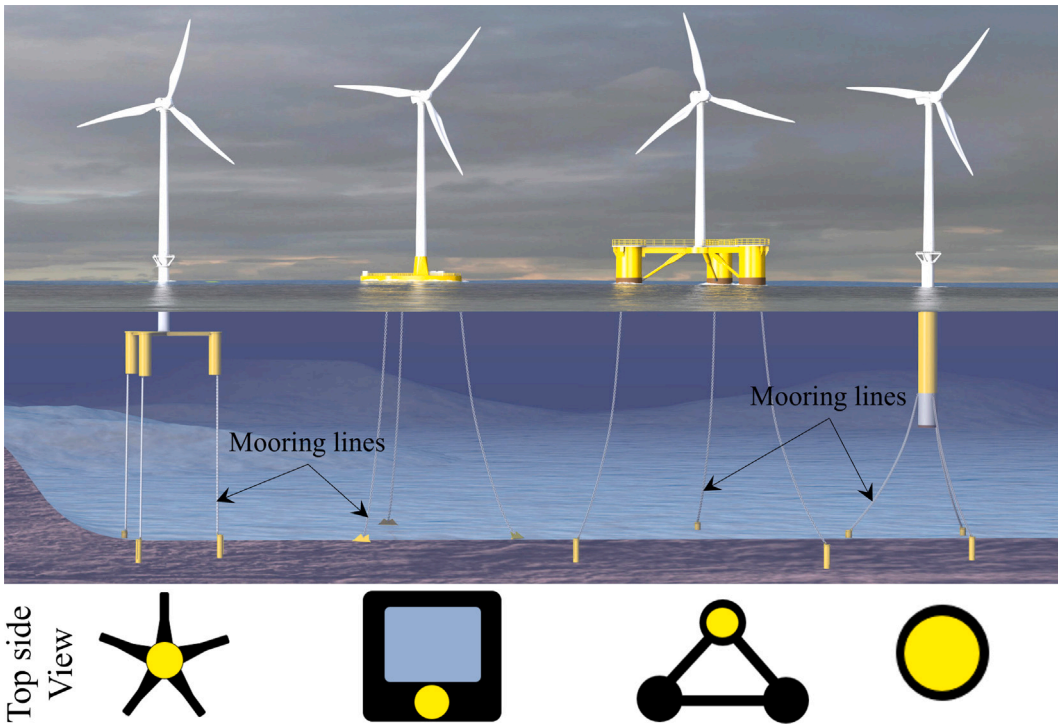

Fig. 1. Types of floating wind turbines showing topside view in black the floating structure and the turbine location in yellow. From left to right: Tension Leg, Barge, Semi-submersible and Spar.
Source: Adapted from [18].

itself [14]. FOWT stability can be achieved through various methods, such as ballast, mooring and buoyancy stabilization [15]. Furthermore, there is an influence of coupled wind and wave loading on the system [1], and of system parameters (such as added damping) on the stability of the floating structure, as previously studied by Tian et al. [16]. The latter stated that added damping makes the system safer by reducing aerodynamic and hydrodynamic loading.

FOWT systems have 6 degrees-of-freedom (6-DOF) *(surge, sway, heave, roll, pitch and yaw)*, with the pitch angle needing to be kept below approximately 10 [deg] of angular displacement during operation for efficient and safe wind turbine performance [2]. Thus, the structure's motion should be evaluated under working and survival conditions to prevent failure under extreme sea scenarios as well as to identify wave conditions permitting an acceptable power output. The typical wave periods used for testing the designs range between 5 and 25 s [1], while the wave heights can vary significantly depending on the global location. For the North Sea case, significant wave heights (Hs) range from 1 to 7 m in winter and are reduced to approximately 1 to 3 m in the summer, with Scottish coast conditions for both seasons depicted in Fig. 2. Other FOWT challenges are associated with technology deployment and maintenance. Some are directly linked to the design of the turbine structure and result in high operation and maintenance costs, that can account for up to 30% of overall cost of energy. Traditionally, offshore wind maintenance operations are performed using jack-up or heavy lift vessels, which are limited to water depths of 60 m. To address this limitation and reduce costs, towing FOWT structures to port for maintenance purposes is proposed as an alternative [17]. Finally, the electrical connection of FOWT poses a challenge, since floating-system motion can fatigue the electrical cable.

This paper addresses the dynamic behaviour of a semi-submersible FOWT concept designed by T-Omega Wind Ltd, the novelty of which relies on its light weight (approximately 80% less steel in its structure) and its single line synthetic mooring (reduced length and cost), leading to an estimated 41% reduction of project capital expenditures (CapEx) [19] to an overall value of $3.3M$ [USD/MW] in a system of 10 [MW] of installed capacity. The system is designed with modular parts and connections in order to ease its manufacture and transportation to or from a port. No crew boarding or maintenance work is planned offshore, instead the turbine will be towed to port (reducing connection/disconnection time from days to hours) for an estimated 45% reduction of Operational Expenditures (OpEx), and hence, to an overall LCOE reduction to 73 [USD/MWh]. The light structure is stabilized and sustained by four hydrostatically stiff interconnected floats providing the concept with a relatively high buoyant natural frequency that allows it to float over severe waves. The concept is initially designed for 10 MW capacity and uses a single line mooring system to provide a weathervane effect, reducing costs related to the mooring system and nacelle yaw drive. Consequently, the mooring (with tension created by wind thrust) generates a negligible restoring torque. Therefore, the yaw motion is ignored at the current stage of this study. The research presented here focuses on the dynamics of the *heave* and *pitch* DOF of the system under hydrodynamic loads only, by modelling the structure and simulating the FOWT behaviour under a wide range of wave conditions. Wind loads acting on the system and system control are neglected in this work to evaluate the hydrodynamic system responses affected by its configuration and validate simulations with experimental data. To study the system behaviour, a detailed CAD model is developed using SolidWorks (see Fig. 5) and simulations are conducted using the Marine Simulator at the National Decommissioning Centre (DNC). The Marine Simulator is a multiphysics integrated software package developed by the Offshore Simulator Centre (OSC) [20], which integrates equations of motion developed by Algoryx to evaluate the hydrodynamic and environmental loads acting on the systems [21]. The model and simulations are validated with experimental tests performed on a 1:60 prototype by the Kelvin Hydrodynamics Laboratory (KHL) at the University of Strathclyde.

This paper summarizes the work undertaken to develop and calibrate the hydrodynamic model of the T-Omega Wind FOWT concept. The subsequent sections are organized as follows: Section 2 explains the methodology used to compute the system dynamic responses, and

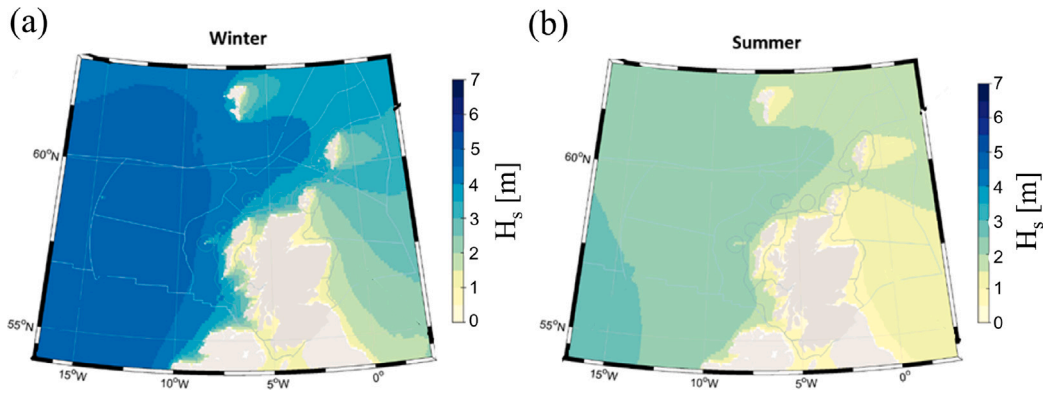

Fig. 2. Average significant wave heights (H_s) in metres for Scottish coastline. (a) Winter wave average heights with a usual significant wave height of 5 m on the Atlantic West coast and 2–4 m along the East coast. (b) Summer wave average heights with a usual significant wave height of 2–3 m on the West coast and 1–1.5 m on the East coast [22].

summarizes the Equations of Motion (EOM) in matrix form incorporating the forces acting on the system. It is followed by Section 3, which describes the 1:60 scale prototype and the experimental tests performed at KHL. Section 4 explains the 6-DOF model used to evaluate system dynamic responses and the calculation of RAOs. Subsequently, Section 5 presents and discusses the simulation results and their validation with experimental data, and introduces an analytical expression for system dynamic responses within the range of the study. Finally, Section 6 summarizes the main research findings and provides ideas for future work.

2. Methodology

The hydrodynamic response of the FOWT concept designed by T-Omega Wind was numerically evaluated with regular waves in order to compare to wave basin experiments. In future, simulations assess the system's dynamics under ordinary and survival sea scenarios with the advantage that the same prototype and virtual environment can also be used to study the dynamics of towing deployment, decommissioning and maintenance operations. This section presents the methodology followed to study the hydrodynamic responses of the system and introduces the state-of-art Marine Simulator emphasizing the environmental loads included in the current model among other loads critical for future studies performed under realistic hydro-aero dynamical studies.

The numerical model is created within the Marine Simulator located at the NDC at the University of Aberdeen. This consists of a 300-degree visual immersive environment with four control stations. It is a real-physics simulator able to evaluate, visualize and collect data from structure-environment dynamic interactions in real time under different sea, weather and dynamic scenarios. This enables position, velocity, acceleration and forces acting on a rigid body to be evaluated. The simulator operates the software FATHOM (OSC developer [20]), which allows user interaction, and is combined with the Algoryx Dynamics [21] algorithm with the Hydrodynamics module for computation of sea-structure interactions. The simulation scenarios and environmental parameters are built in the Sandbox software, which is responsible for the real-time visualization and handling of control signals. In Fig. 3 we depict the marine simulator workflow.

Algoryx utilizes a triangle meshed CAD model [12] to evaluate local hydrodynamic, hydro-static and added environmental loads, that are then integrated over the bodies surface for application to the 6 DOF of each rigid bodies' floating or submerged in the sea environment. Fig. 5 shows a schematic example of forces acting on each surface element. The equations of motion (EOM) for each object placed in the scene (four floats interconnected, turbine structure, three blades and a generator) are expressed by Eq. (1) as follows,

$$[M]\{\ddot{\mathbf{a}}\} + [C]\{\dot{\mathbf{a}}\} + [K]\{\mathbf{a}\} = \{\mathbf{F}\}, \tag{1}$$

where $\mathbf{a}$ contains the 6 DOF vector of time dependent state variables denoted as $\{\mathbf{a}\} = \begin{bmatrix} x(t) \\ y(t) \\ z(t) \\ \varphi_x(t) \\ \varphi_y(t) \\ \varphi_z(t) \end{bmatrix}$, where $x(t)$, $y(t)$ and $z(t)$ are the surge, sway and heave displacements, while $\varphi_x(t)$, $\varphi_y(t)$ and $\varphi_z(t)$ denote roll, pitch and yaw orientations, as depicted on the wind turbine model schematic in Fig. 5(a). M is a matrix of coefficients containing the inertia and the added mass terms, C contains the linearized viscous damping coefficients (gyroscopic phenomena are not included) and K the stiffness coefficients between coupled bodies. Since the simulator considers objects as rigid bodies, the stiffness matrix K will contain mechanical, hydrostatic and mooring interactions between the multiple bodies making up an assembly. All external hydrostatic, hydrodynamic and mooring forces are included in the $\mathbf{F}$, where the zeroth and first-order contributions are the buoyancy force, F_b (Eq. (2)), drag force (F_{Drag}) and lift force (F_{Lift}) expressed in Eqs. (3)–(4) as follows,

$$F_b = -\rho g \iint_{Sb} h\hat{\mathbf{n}}\, dS, \tag{2}$$

$$F_{Lift} = -\iint_{Sb} p\,\hat{\mathbf{n}} \cdot \hat{\mathbf{k}}\, dS, \tag{3}$$

$$F_{Drag} = -\iint_{Sb} p\,\hat{\mathbf{n}} \cdot \hat{\mathbf{i}}\, dS + \iint_{Sb} \tau\,\hat{\mathbf{n}} \cdot \hat{\mathbf{i}}\, dS, \tag{4}$$

where ρ and g are the density of fluid and gravity, respectively. Here, S_b represents the submerged surface area, p is the hydrostatic pressure applied on the structure submerged area, which depends on the fluid density and the sea water level and τ is the shear stress distribution acting on the submerged body surface, $\hat{\mathbf{n}}$, $\hat{\mathbf{k}}$ and $\hat{\pi}$ denote the unit vector normal to the surface, vertical and parallel to the fluid velocity, respectively. Moreover, first and second order hydrodynamic forces are also included in the force matrix. The software incorporates current and wind loads acting on the bodies, which are evaluated as a polynomial function of the relative velocity between the body and the velocity field considering viscous and internal forces, as in Eq. (5) [23],

$$F_{Current/Wind} = C_t(\varphi_z)V_r + C_{t+1}(\varphi_z)V_r^2, \tag{5}$$

where V_r is the relative velocity between the body and the field and C_t denotes the damping for a time t. Note that current and wind loads are not considered in the investigation presented in Sections 4 and 5. Furthermore, the inertia forces considered are the radiation, incident wave (Froude–Krylov) and wave diffraction forces, which are dependent on the fluid velocity potential $\phi(t) = \phi_R(t) + \phi_I(t) + \phi_D(t)$ and are solved by bidirectional interpolation. The radiation force has a memory effect that is critical for the convolution $\mathbf{F}$ term in the time domain under the case of irregular waves. Since this study focuses on

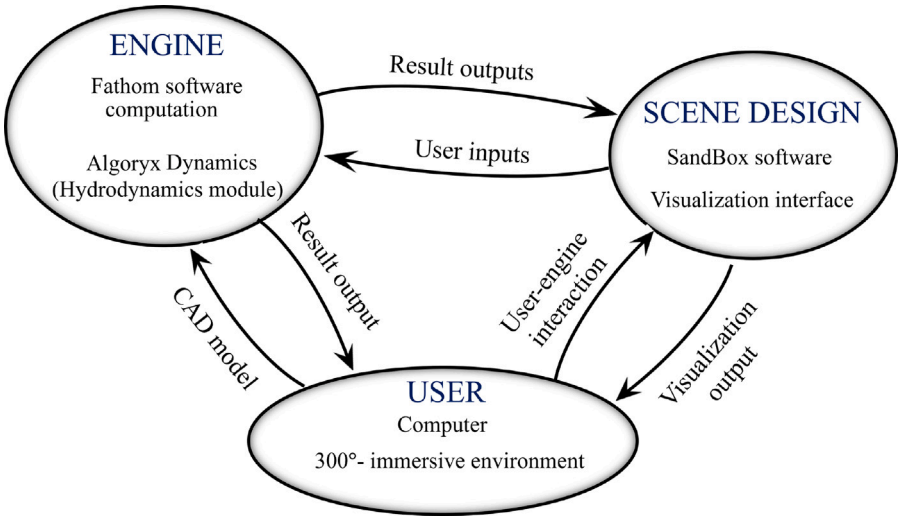

Fig. 3. Marine Simulator software and hardware integration workflow.

the regular wave case, the radiation memory effect is not considered in this study. Hence, the forces are expressed in Eqs. (6)–(8) as follows,

$$F_R = -\iint_{Sb} \rho \left(\frac{\partial \phi_R}{\partial t} \right) \hat{\mathbf{n}}\, dS, \tag{6}$$

$$F_I = -\iint_{Sb} \rho \left(\frac{\partial \phi_I}{\partial t} + gz \right) \hat{\mathbf{n}}\, dS, \tag{7}$$

$$F_D = -\iint_{Sb} \rho \left(\frac{\partial \phi_D}{\partial t} \right) \hat{\mathbf{n}}\, dS, \tag{8}$$

where z denotes the vertical position of the body CG and ϕ_R, ϕ_I and ϕ_D represent the radiation, incident and diffraction fluid velocity potential, respectively. Note that in Eq. (7), $\rho \frac{\partial \phi_I}{\partial t}$ represents the hydrodynamic pressure that only exists if waves are present.

Second-order wave forces are considered in the FATHOM HYDRO algorithm [23]. The generated nonlinear loads [24], which are the second order terms, are solved with the Quadratic Transfer Function (QTF). Moreover, for the case of semisubmersible floating structures, the first-order mean drift force and second-order slow varying drift force have an impact on the response [25]. Hence, they are considered in the algorithm and they are expressed with Eq. (9) [26] as follows,

$$\begin{aligned} \vec{F}^2 = & -\oint_{WL} \frac{1}{2} \rho\, \xi_r^{(1)} \cdot \xi_r^{(1)}\, \hat{\mathbf{n}}\, dL + \iint_{Sb} \frac{1}{2} \rho \left| \nabla \phi^{(1)} \right|^2 \hat{\mathbf{n}}\, dS + \\ & + \iint_{Sb} \rho \left(a \cdot \nabla \frac{\partial \phi^{(1)}}{\partial t} \right) \hat{\mathbf{n}}\, dS + M_s R \cdot \ddot{a} + \iint_{Sb} \rho \frac{\partial \phi^{(2)}}{\partial t}\, \hat{\mathbf{n}}\, dS, \end{aligned} \tag{9}$$

where $\xi_r^{(1)}$ denotes first order wave elevation, $\phi^{(1)}$ and $\phi^{(2)}$ denote first- and second-order velocity potential, a is the body position, ä the acceleration of the CG and M_s denotes the mass of the floating body, while WL is the waterline and R is the rotation matrix. The first four terms of the equation represent the mean drift force evaluated with the first-order solution while the last term defines the slow drift force. For computational simplification the algorithm applies Newman's approximation [27] to evaluate the QTF [28]. Furthermore, to define accurate system damping behaviour in cases of aperiodic motion generated by non-environmental external forces acting on the system, the Marine Simulator adds frequency-independent damping forces or torques (F_{fi}) to the system. Representative examples where these forces are applied are manoeuvring and heeling procedures (i.e. a tug induces external forces on the 6 DOF of the system while towing or connecting both systems). For these cases the damping can be specified on the force application DOF direction and the coupling relationship type between the system DOFs. The extra force terms are body-velocity dependent and are calculated as in Eq. (10) [23],

$$F_{fi} = C\,[V_i \cdot V_{i+1} \cdot \cdots \cdot V_n], \tag{10}$$

where n is the number of coupling effects, C denotes the damping coefficient for the added force and the sequence of V_n multipliers represent the first- or second-order damping force/torque terms exerted to each degree of freedom. V_i multipliers are expressed as $\dot{V}_{[a]}$ if they are first-order terms and expressed as $\dot{V}_{[a]}^2 \cdot sgn\left(\dot{V}_{[a]}\right)$ in case of second-order terms, where [**a**] denotes the DOF and $\dot{V}$ denotes system's velocity. These frequency-independent forces are neglected by the model since no cases of non-environmental forces are considered when evaluating the influence of wave excitation. Although, continuation studies on system reliability in towing and manoeuvring scenarios will require inclusion of those terms.

The next section presents the scaled experimental prototype with its system components and characteristics. Scaling principles are outlined, then experimental set-up and tests undertaken are explained.

3. Experimental set-up and studies

An experimental model was developed for T-Omega Wind Ltd by Kelvin Hydrodynamics Lab (KHL) at the University of Strathclyde to study the dynamic responses of the novel floating wind turbine under different scenarios. Trials conducted to date involved a non-moored, non-operating system with soft station-keeping restraint at two levels of ballast. RAOs were measured at different wave heights, and a few extreme sea states were also evaluated. The floating structure was geometrically scaled to 1:60 of the full size with 120 [m] hub height, and comprises a buoyant platform, four support legs converging on a hub and three non-rotating horizontal axis blades (not used in tests). The weight of the turbine nacelle assembly is added at the top of the structure so stability can properly be assessed. The fibreglass platform is comprised of four cone-shaped shallow-draft floats braced together, with sufficient hydrostatic stiffness to generally follow the water surface elevation [29]. It provides four points of support for the turbine structure made from carbon fibre tubes. Fig. 4(c) shows the components of the test model, and technical specifications are presented in Table 1. The model is excited either by periodic waves with specified height and period, or by a JONSWAP sea state of specified T_p, H_s, and γ. The KHL tank has dimensions $76 \times 4.6 \times 2.3$ [m] in length, width and depth. Four paddle-type active absorbing type wave makers generate the required waves (<0.6 [m] for regular waves and <0.5 [m] for irregular waves), and a passive-type wave beach of 13.5 [m] of length located at one end of the tank absorbs incoming waves with a reflection coefficient below 5%, as shown in Fig. 4(a–b).

During the tests, the floating turbine model was located 32 [m] from the wave maker and the 6 DOF displacement of its CG is monitored with

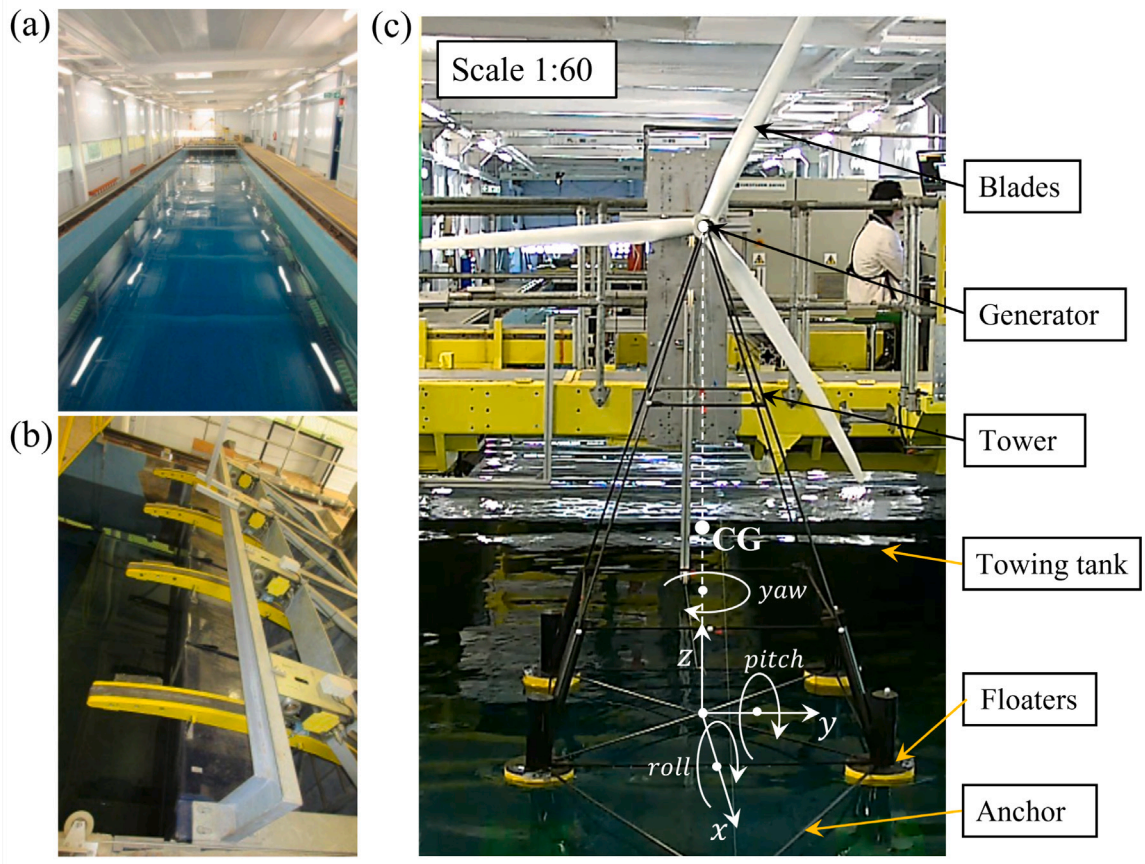

Fig. 4. (a) Towing tank tests at the Kelvin Hydrodynamics Laboratory. (b) Wavemaker paddles for wave frequency and amplitude generation. (c) Experimental test rig of novel floating wind turbine designed by T-Omega Wind in a towing tank showing its main components.

Table 1
Scaled model technical characteristics.

Model characteristics	Light displacement condition
Scaled mass [kg]	4.36
Vertical position of CG [m]	0.94

Table 2
Tests performed.

Sea state	Full scale wave heights [m]	Full scale wave periods [s]
Low	[1,2]	[4–28]
High	[4,6,8,10,12]	[7–25]

a Qualisys optical motion capture system. The system was restricted in the wave propagation direction between a pair of taut low-stiffness mooring lines (stiffness = 1.2 [N/m]) so that the model remains near a desired position. To evaluate the hydrodynamic behaviour, regular waves of various amplitude and frequency were used with Froude scaling as recommended by Chen et al. [30] and Cao et al. [31] and shown in Eqs. (11)–(12) for the ranges of wave height and period presented in Table 2.

$$T_{full\ scale} = T_{tank}\ \sqrt{s}, \tag{11}$$

$$H_{full\ scale} = H_{tank}\ s, \tag{12}$$

where T and H denote wave period and height, while s is the geometrical scale factor (of value 60). Free decay tests, regular waves, sea state waves and qualitative dropped-weight "Wind Gust" tests were performed. This paper focuses on the dynamic response of the wind turbine model under two types of Sea States (*"Low"* and *"High"*) and hence, only regular wave results are presented. Seven combinations of wave period and height tests were used for this research, performed with ballasted and unballasted floats showing an almost identical system response. For comparison to simulations in this paper, only the unballasted test conditions are considered.

This section presented the 1:60 scaled model and experimental setup of the FOWT model and the overview of experimental tests performed. In the next section we introduce in detail the digital model of the floating wind turbine and its validation against the experimental data obtained at KHL.

4. The model

A full-scale T-Omega wind FOWT novel concept model described in Section 3 is implemented as a SolidWorks CAD model. It comprises four interconnected buoyant conical floats providing four points of structure support, along with a cable-braced 'standoff' to support the mooring point. The system structure or "Tower" is composed of a hollow tube frame allowing the system to be lightweight without compromising robustness. For cosmetic purposes three non-rotating blades are sometimes joined to the top, though not during trials. Each of the first three components (rotor not modelled) is a 6 DOF subsystem within the Simulator software, hence, the entire system would contain 18 DOF that allow the feasibility of the design concept at its current stage to be validated hydrodynamically. However, the high connection stiffness between components permits the system to be treated as a rigid body with overall 6 DOF and eliminating K terms due to rigidity. Thus, the general equation applied to each system component can be simplified to a single equation applied to the rigid body expressed in Eq. (13),

$$[M]\{\ddot{\mathbf{a}}\} + [C]\{\dot{\mathbf{a}}\} = \{\mathbf{F}\}, \tag{13}$$

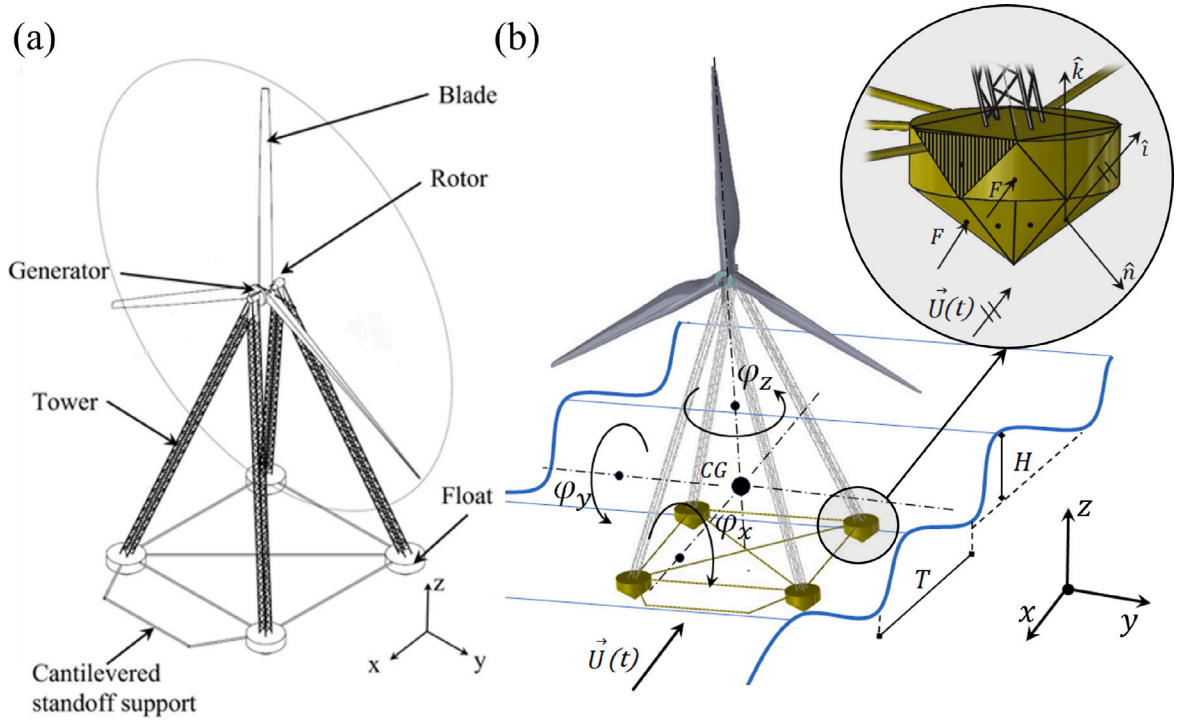

Fig. 5. T-Omega Wind full scale CAD model of 6 degrees of freedom. (a) Model components including a cantilevered standoff support comprising 4 floats, the tower as supporting structure, a generator and 3 blade rotor. (b) Schematic model-sea interaction and floats triangular mesh. (The mooring system is a single connection in the floating support with no obvious dynamic effects under unidirectional waves).

Table 3
Component masses used to adjust CG position of the initial full scale model iteration of FOWT. T-Omega Wind subsequently revised the design with altered base dimensions [29] and 50% greater mass (still far lighter than conventional FOWT).

Components	Mass [t]
Tower	296.2
Cantilevered standoff support +4 floats	503.8
Generator	140
3 blade rotor	60

where **a** denotes the 6 DOF vector of time dependent state variables of the rigid body ("Tower" and floats substructure). The overall system embodies the masses of the individual components, and therefore correctly captures the overall system CG. This study considers a CG located at 56 [m] from the base and a pitch radius of gyration of 69 [m]. Table 3 presents the masses of each component considered in the model.

The CAD model is imported into the simulator, where it is meshed to apply the forces acting on each triangular cell. The model's displacement is restricted in the y direction (orthogonal to wave direction) as well as around its yaw axis z, to match experimental tests, which showed that these displacements can be neglected due to their very small values. When modelling the turbine operation, the turbine mooring system is considered as a single mooring point of connection in the standoff support, which provides a weather vane effect to the system. Although, the effect generated in the system's heave and pitch DOF will not be obvious when the system is investigated under unidirectional regular waves. Since the study concerns only the dynamic responses of the FOWT when the blades are static, the simulations and experimental studies are performed with the rotor mass lumped into the system's mass and inertia to identify wave parameter ranges where the body exhibits highest heave and pitch responses.

4.1. System evaluation and model adjustment

To study the FOWT dynamic response under varying regular waves, *Response Amplitude Operators (RAOs)* are computed for heave and pitch directions for the four-float assembly (see Fig. 6(a)). Previous authors have described several forms of a system RAO evaluation with different mathematical methods [32–34]. For this study, these are approximated as a ratio between the maximum amplitudes of system's displacement and the periodic wave amplitude of excitation for a specific wave period, which represents the relationship between the system motion range and the excitation wave height. These can be translated into the relation between the peak-to-peak amplitudes of the system's response and the excitation wave height, as depicted in Fig. 6(b) and described by Eq. (14) for each DOF,

$$RAO \approx \frac{A_{[\mathbf{a}]}}{A_{wave}}, \tag{14}$$

where $A_{[\mathbf{a}]}$ denotes the mean response amplitude without transition phase for each degree of freedom and A_{wave} is the periodic wave amplitude.

To evaluate the dynamic responses of the system, the trajectory and velocity time histories are evaluated and compared with the experimental results by applying Froude scaling. Fig. 7(a–d) presents examples of heave and pitch time histories for 2 [m] wave height (periods of 10 and 14 [s]) and Fig. 7(e–f) an example for 12 [m] wave height (period of 20 [s]), where simulation results (blue colour) are in close agreement with the experiment (red colour) results. The system nonlinearities produced by second order forces are evaluated with the approximations presented in Section 2 (See Eq. (9)). Thus, the model is calibrated, with the experimental data summarized in Section 3. By adjusting the floats' coupled damping coefficients in the heave and pitch directions in the marine simulator, as previously mentioned by Skandali et al. [32], the model can match amplitude experimental results from the wave tank. To achieve this, damping coefficients in $[C]$ matrix, (C_{33}) and (C_{55}) are defined via 6 non-dimensional damping ratios $[D_i]$. A change in the

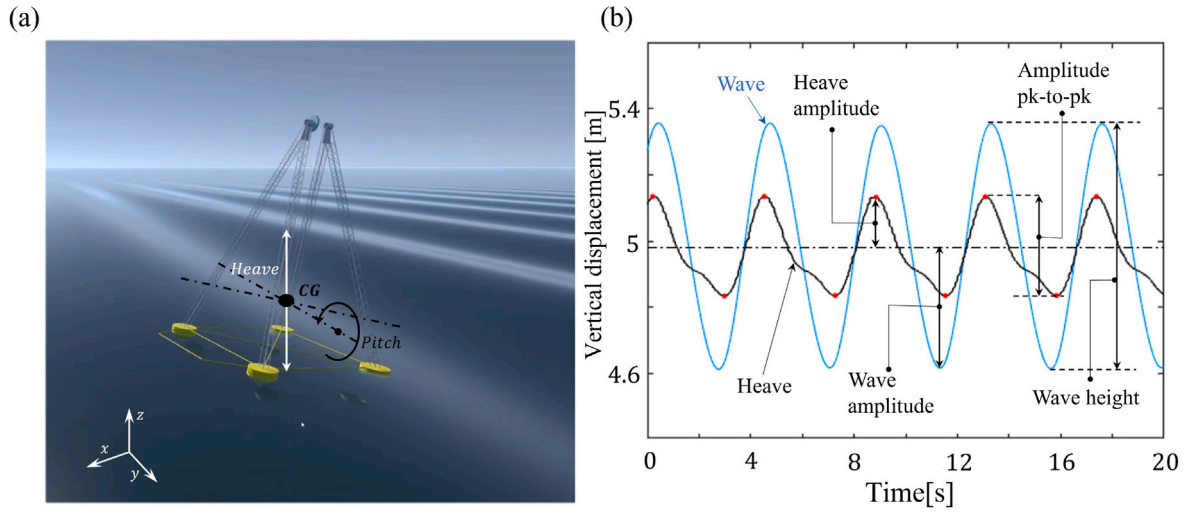

Fig. 6. (a) The model comprised of floats and support tower used to evaluate system RAOs for heave and pitch under periodic wave excitation. (b) An explanatory graph of RAO evaluation showing vertical displacement time history of FOWT structure (black) under periodic wave excitation (blue), maximum and minimum displacements are represented with red points.

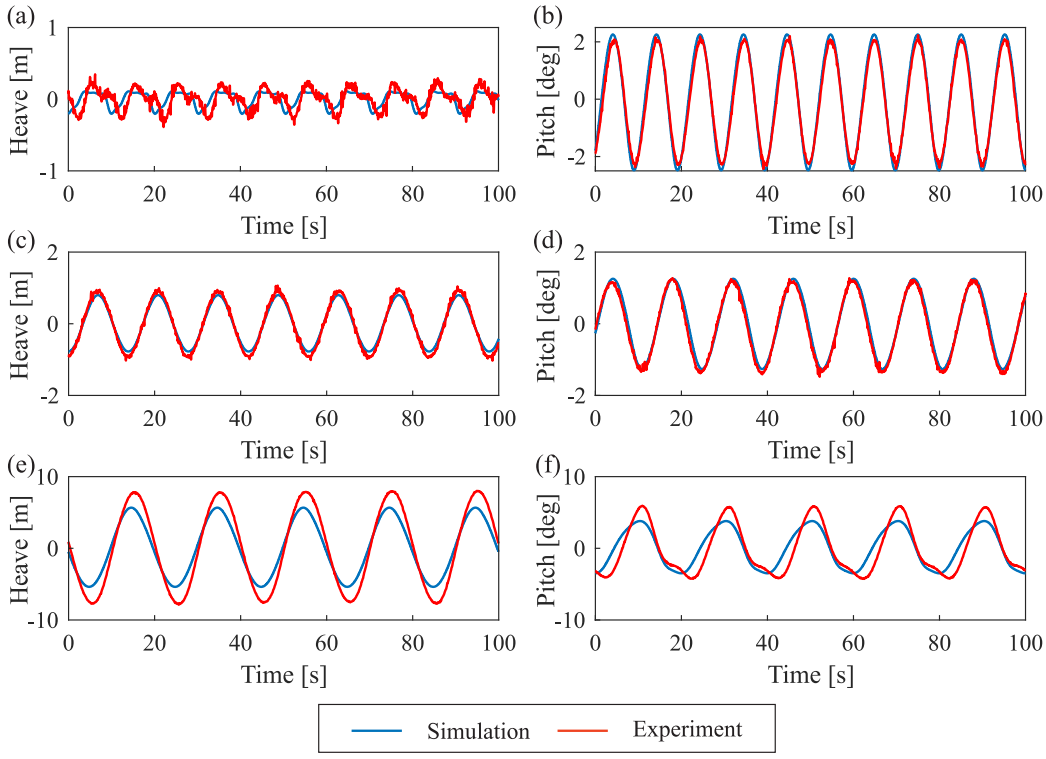

Fig. 7. Comparison between the experimental (red colour) and simulated (blue colour) time histories of the FOWT heave and pitch displacements. (a–b) T = 10 [s] and H = 2 [m], (c–d) T = 14 [s] and H = 2 [m], (e–f) T = 20 [s] and H = 12 [m]. Exemplary video showing the recording from the wave tank and the Simulator for the case shown in panels (e–f) is available in the supplementary material of this paper.

damping ratio for a given DOF, varies a corresponding entry of the C matrix, e.g., $C_{ii} = 2D_i\omega_{oi}M_{ii}$, where ω_{oi} denotes the natural frequency of each degree of freedom and M_{ii} is the corresponding component of the inertia matrix (i.e. for heave DOF $C_{33} = 2D_3\omega_{o3}M_{33}$). Note that the non-dimensional damping coefficients adjusted in this study are D_z and D_{φ_y} referred to henceforth as heave and pitch damping, respectively.

The following section presents the heave and pitch RAOs obtained from the simulator which were calibrated for *"High"* and *"Low"* wave excitation height ranges and the corresponding selected damping parameters.

5. Results and discussion

The floating sub-structure of the novel FOWT designed by T-Omega Wind is evaluated in the marine simulator under regular-wave excitation by changing the wave height (H) and period (T). Then, heave and pitch RAOs are evaluated to investigate vertical displacement and angular orientation for periods of wave excitation from the interval $T \in [4.5\text{–}28]$ [s] in two distinguished *Sea States* ranges: *"Low Sea State"* for wave heights $H \in [1\text{–}2]$ [m] and *"High Sea State"* for wave heights $H \in [4\text{–}12]$ [m]. All simulations are calibrated in the marine simulator

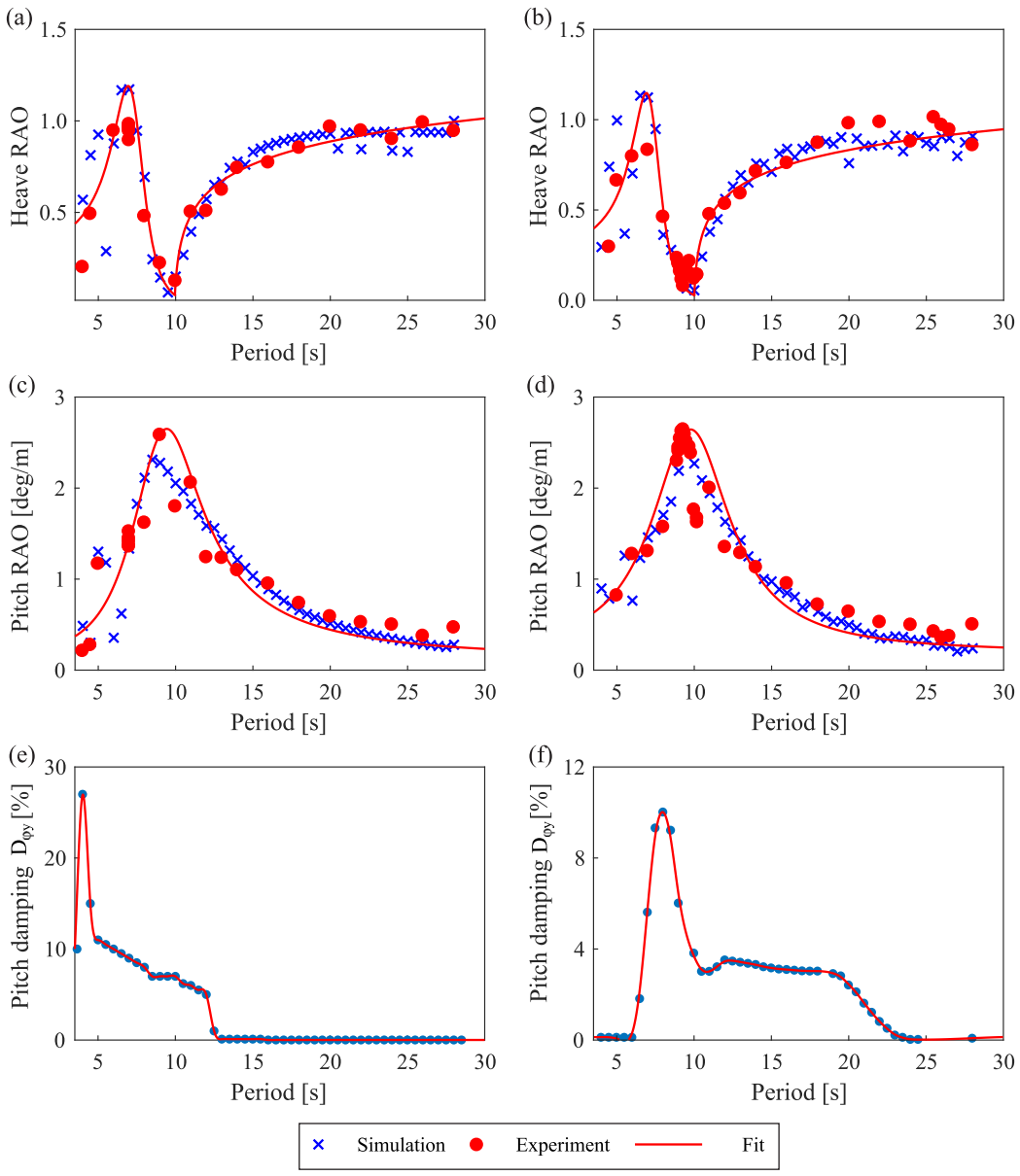

Fig. 8. Model validation for *"Low Sea States"* with comparison between the Simulation (blue colour) and the experimental (red colour) heave and pitch RAOs float responses for periodic waves within the range of $T \in [5\text{–}28]$ [s] after pitch damping ratio adjustment. (a–c) $H = 1$ [m] and (b–d) $H = 2$ [m]. Non-dimensional pitch damping adjustment [%] for coupled heave and pitch responses in (e) $H = 1$ [m] and (f) $H = 2$ [m]. (See Appendix B for responses fit parameters).

by varying the coupled floating sub-system damping for heave and pitch DOF and comparing against the experimental data. The values of adjusted damping ratios are presented in this section for each wave height and period considered. In a sea state consisting of many wave periods, it is proposed that the damping coefficient corresponding to the peak spectral period would be used.

Heave and pitch RAO simulation results for *"Low Sea States"* as a function of wave excitation and their comparison with experimental results are shown in Fig. 8(a, c) and (b, d) for wave heights of 1 and 2 [m], respectively. The system's heave natural period is observed at 6.5 [s] and the pitch natural period is observed at $T = 9.5$ [s] for $H = 1$ [m] and $H = 2$ [m], where a maximum value of pitch angular displacement coincides with the absolute minimum value for heave vertical displacement in the range of studied wave period. Similar behaviour has been reported by [35]. At the pitch natural period for a wave height of $H = 1$ [m], the minimum value of heave RAO recorded is 0.05, which is directly related to the wavelength and float spacing of 70 [m] and corresponds to one of the floats being at the wave peak and other at the wave trough. The latter value corresponds to a CG vertical displacement of 0.05 [m] and the maximum pitch RAO value recorded is 2.5, which translates to an angular deviation of 2.5 [deg], that is also related to the FOWT pitch when one float is at the wave peak and other at the trough. For $H = 2$ [m] case, the minimum value of heave RAO is 0.05, which corresponds to a vertical displacement of 0.1 [m] and the associated maximum value for pitch RAO is 2.6 [deg/m], which corresponds to a maximum angular displacement of 5.2 [deg]. Furthermore, for both cases the heave RAOs present a relative maximum vertical displacement for wave periods in the range of $T \in [6.5\text{–}7]$ [s]. The maximum simulation heave RAOs recorded are 1.18 and 1.15 for $H = 1$ and $H = 2$ [m], respectively, which correspond to 1.18 [m] and 2.3 [m] of CG vertical displacement and heave resonant period of $T = 6.5$ [s]. As the period increases, the heave RAOs decrease drastically reaching their minimum values at the pitch resonance period, where it starts increasing logarithmically until

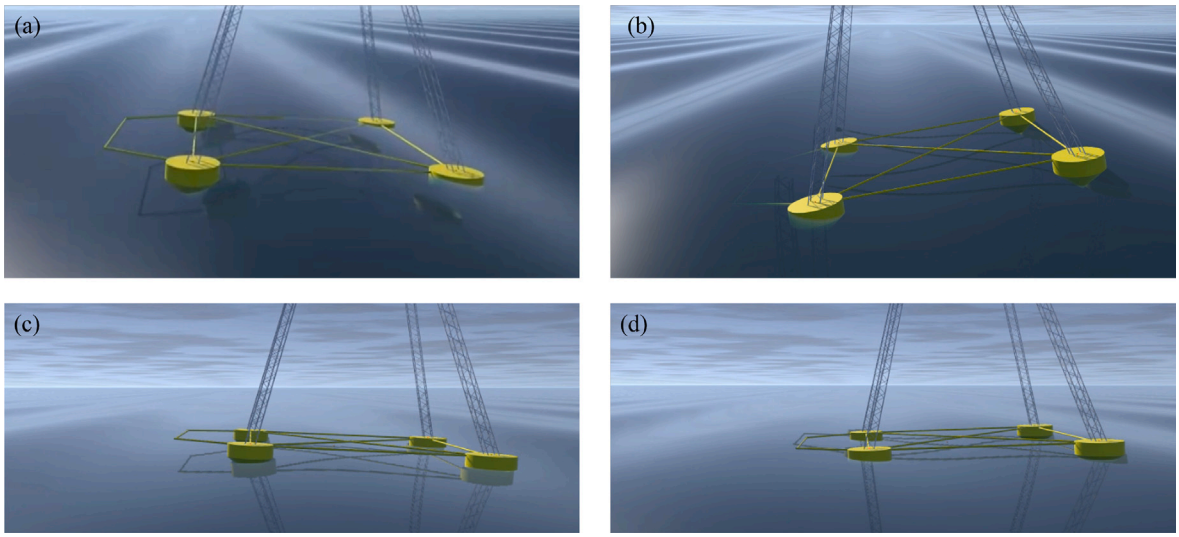

Fig. 9. Selected maximum pitch displacements of system under *High* and *Low* Sea States under regular excitation. (a–b) Regular waves of $H = 8$ [m] and $T = 10$ [s] (resonance period), where less volume of front and rear floats is submerged for the maximum pitch displacement. (c–d) Regular waves of $H = 2$ [m] and resonance period of $T = 9.5$ [s], where the floats waterline is almost kept constant during the excitation period.

it settles after $T \sim 15$ [s] to reach a heave RAO of ~ 1 at $T \sim 25$ [s]. Similar results have been presented previously by [36] for a Spar FOWT design. In addition, pitch RAO results follow a "bell" shaped trend for both cases. For low wave periods of $T \sim 5$ [s] pitch RAOs are less than 1 [deg/m] for $H = 1$ [m] and less than 1.5 [deg/m] for $H = 2$ [m]. As wave period increases, the resonance period is reached with their maximum to start decreasing asymptotically until reaching approximately $T \sim 25$ [s] with a pitch RAO of 0.45 [deg/m] corresponding to 0.45 [deg] and 0.90 [deg] for $H = 1$ [m] and $H = 2$ [m], respectively. The FOWT's motions may affect the system aerodynamic performance and power output [37], especially for large pitch acceleration which produce great blade inertia loads [38]. In this research, for both considered cases of *Low Sea States* all pitch displacement values recorded are less than 10 [deg]. Therefore, for cases when $H \in [1–2]$ [m] within the range of periods studied, the system responses lie on the pre-established range of acceptable system motion limit values [2]. For *"Low Sea States"* only the pitch damping coefficient need be adjusted to obtain a good agreement between the simulation and experimental results. Hence, the heave damping ratio is maintained at a value of $D_z = 0.1\%$ and pitch damping coefficient values as a function of wave period are shown in Fig. 8(e) and (f) for wave height cases of $H = 1$ [m] and $H = 2$ [m], respectively.

A similar procedure of damping coefficient adjustments is followed for *"High Sea States"* by adjusting the floats' heave and pitch damping ratio. A set of wave height cases of $H = [4, 6, 8, 10, 12]$ [m] are selected and simulations are performed for selected wave periods of $T \in [4.5–26]$ [s]. The results are validated with the experimental tests presented in Appendix A. Simulation results for *"High Sea States"* display heave and pitch RAOs results that can be considered identical. Thus, a trend is identified for wave period dependence. All cases depict a pitch resonant period at $T = 10$ [s], where heave RAO ~ 0.2 and pitch RAO ~ 1.55 [deg/m]. The heave resonance period is identified at $T = 7$ [s] with a approximate value of heave RAO of 0.86 and for greater periods of $T > 15$ [s], the heave RAO simulations start stabilizing reaching 1 at $T \sim 25$ [s]. From the pitch RAO results, the wave parameter ranges, for which the system presents higher pitch deviation than 10 [deg] are identified. For the cases of $H = 4$ and $H = 6$ [m] the system would have a better performance when $T \in [4.5–25]$ [s], whereas the system experiences larger amplitudes of pitch motion (>10 [deg]) for $H = 8$ [m] at approximately $T \in [6.5–13.5]$ [s], $H = 10$ [m] at approximately $T \in [7.0–11.5]$ [s] and $H = 12$ [m] at approximately $T \in [6.5–12.5]$ [s]. Results showed that even under larger amplitudes of deviation, the device is able to return to its equilibrium position, allowing the device to withstand harsh environmental conditions by entering a safe survival mode. Since from wave heights greater than 6 [m] the weather conditions could have put the turbine into a parked status (survival mode), the pitch deviation angle greater than 10 [deg] would not have an impact on the device's power production. Simulation results for *"High Sea States"* are presented in Fig. 10(a) for the heave RAOs and in Fig. 10(b) for the pitch RAOs depicted as solid lines. A similar dependence on wavelength can be identified for both *"High"* and *"Low"* (dashed lines) *Sea States* scenarios. Moreover, in some cases simulation and experimental results present non-simple harmonic responses of the pitch angular displacements, as depicted in Fig. 7(b). This behaviour is caused by the geometrical nonlinearities induced by the combination of conical and cylindrical shaped floats, which does not maintain a constant water plane area under system excitation. This effect is particularly noticeable for larger wave heights. Fig. 9 shows selected simulation scenarios, where due to the vary large amplitude of the excitation, less of the float is submerged. For *"High Sea States"* of $H = 8$ [m] and turbine's resonance period ($T = 10$ [s]) the simulation response presents this behaviour induced by the geometrical nonlinearities. Therefore, Fig. 9(a–b) shows the simulation instant of velocity reversal. In contrast, Fig. 9(c–d) depicts the opposite case for $H = 2$ [m] and resonance period of $T = 9.5$ [s], where the conical shape of the floats almost stay submerged at any stage of excitation.

The former observation and the strong similarity of RAO dependence on wave period for *"Low"* and *"High"* *Sea States* allow us to formulate analytical approximations to the RAOs, to supplement the limited experimental data available for those cases. Fig. 10(a–b) shows the simulated RAO results for heave and pitch for all cases considered (*Low Sea States* depicted with dashed lines), where each set of results is evaluated for discrete periods and the continuity trend is predicted with the spline interpolation. Fig. 10(c–d) depicts the corresponding RAOs fits for heave and pitch for *Low* (red) and *High* (black) *Sea States* and Fig. 10(e–f) depicts the corresponding damping coefficient variation for heave and pitch used in the simulations, respectively. The equations describing the trends can be expressed analytically by Eq. (15) for the heave RAO, which is a combination of a tilted Lorentzian distribution [39] joined to a logarithmic curve, and in Eq. (16) for the pitch RAO responses by using the same tilted Lorentzian formulation

as follows,

$$RAO_{Heave}(T) = \begin{cases} \frac{2A/\pi b'}{1+4\left[\frac{T-X_o}{b'}\right]^2} + e \;\; \forall \;\; T \leq R \\ \\ ln(T-f)d + c \;\; \forall \; T > R \end{cases}, \tag{15}$$

$$RAO_{Pitch}(T) = \frac{2A/\pi b'}{1+4\left[\frac{T-X_o}{b'}\right]^2} + e, \tag{16}$$

where R is the identified pitch resonance period, A denotes the area underneath the fit, X_o is the centre of the maximum peak, e is a fit coefficient and f, d and c are the coefficients adjusted to the data. The tilted angle of the Lorentzian is given by b', and expressed in Eq. (17),

$$b' = \frac{2b}{1+exp\left\{\alpha(T-X_0)\right\}}, \tag{17}$$

where b denotes the full Lorentzian width at the half height of the maximum and α is the tilting angle coefficient. Utilizing these equations, good fits for the heave and pitch RAOs are obtained for *"High"* and *"Low"* sea states respectively and presented in Table 4. From these analytical expressions it is possible to obtain the appropriate damping coefficient for heave and pitch RAOs for any intermediate or close values of wave height and period. This provides an appropriate optimized damping for any periodic wave parameter within the range of the study. The procedure is applied for the 12 [m] wave height presented in Fig. 10, which is also validated with experimental results. Fig. 11(a–b) show the pitch and heave RAOs simulation results obtained from *"High Sea States"* fit for the case of $H = 12$ [m] and $T \in$ [4.5–28] [s] and its validation with experimental data (marked with red points). A comparison between experiment and simulation for the case of $H = 12$ [m] and $T = 20$ [s] is depicted in Fig. 11(c–d), where the former shows the experiment performed in the towing tank and the latter depicts the simulation result computed for the same wave parameters utilizing the floats damping coefficient function obtained for *"High Sea States"* fit. Both images show similarities in the system responses and displacement time histories for this case were previously shown in Fig. 7(c) (A video showing comparison between experiment and simulation for this case is available in the supplementary material). Hence, the proposed method appears to be valid for this system.

This section presented simulation results of the novel concept of FOWT designed by T-Omega Wind performed with the marine simulator under different sea wave scenarios. Results were validated and allowed us to propose generalized approach for RAO modelling for that structure. Final conclusions are summarized in the next section, where the key findings and outcomes of this paper are highlighted.

6. Concluding remarks

The dynamic responses and stability of a novel concept of FOWT, designed by T-Omega Wind, are investigated in this work under different sea state scenarios with a model implemented in a real-physics marine simulator at the NDC. The concept comprises a floating lightweight structure, which employs approximately 80% less structural steel in comparison with a conventional semi-submersible FOWT, supported by four conical shaped floats, which helps the system to glide over waves in harsh marine environments as a result of its high heave and pitch natural frequencies. This unique configuration allows the system to effectively harness wind energy in water depths exceeding 30 [m], with the ultimate goal of tapping into wind energy resources in depths exceeding 60 [m], where conventional fixed platforms are economically unfeasible. The utilization of a single mooring line eliminates the need for a nacelle yaw drive since the restoring force about the mooring point is zero by using the weathervane effect, and substantially reduces mooring costs due to lower marine infrastructure demand compared to other FOWT designs. Furthermore, its shallow-draft design makes it possible to tow the floating turbine to shallow water ports for deployment, maintenance and decommissioning, reducing the cost of those operations by approximately 45% of OpEx.

Table 4
Heave and pitch RAOs equation's fit parameter values for *"Low"* and *High Sea States* (Eqs. (15) and (16)).

Low Sea State					
Heave RAO fit				Pitch RAO fit	
Parameter	Value	Parameter	Value	Parameter	Value
A	25.2	f	8.999	A	26.0
X_o	5.8	d	0.257	X_o	10.0
e	−0.95	c	0.292	e	0.20
b	8.0			b	7.9
α	0.25			α	−0.15
$R = 9.5$					
High Sea State					
Heave RAO fit				Pitch RAO fit	
Parameter	Value	Parameter	Value	Parameter	Value
A	9.3	f	9.637	A	24.4
X_o	6.8	d	0.414	X_o	10.7
e	−0.30	c	0.217	e	0.20
b	5			b	10.8
α	0.10			α	−0.12
$R = 10$					

A full scale 6 DOF model is used as a virtual prototype in the marine simulator to predict system motion response under periodic waves by varying the height (H) and the period (T), which in turn provide heave and pitch displacement system responses. The model CG is adjusted with the sub-component masses to maintain a low vertical CG and improve stability, while individual components of the assembly are connected with high stiffness bracing. Simulation RAO responses for heave and pitch displacements are evaluated against wave period for two different sets of sea states, *"Low Sea States"*, where $H \in$ [1–2] [m] and *"High Sea States"*, where $H \in$ [4–12] [m] for a range of discrete wave periods of $T \in$ [4.5–26] [s]. Consequently, heave and pitch natural periods for the system first design iteration are identified for *"Low Sea States"* at $T = 6.5$ [s] and $T = 9.5$ [s], respectively and for *"High Sea States"* they are identified at $T = 7$ [s] $T = 10$ [s], respectively. Thus, ranges of parameter values where the system presents higher pitch amplitudes than 10 [deg] are only observed for waves of $H = 8$ [m] when $T \in$ [6.5–13.5] [s], $H = 10$ [m] when $T \in$ [7.0–11.5] [s] and $H = 12$ [m] when $T \in$ [6.5–12.5] [s]. The latter cases correspond to extreme sea state scenarios, where the system would enter in parked status mitigating any impact on the system normal performance when pitch displacement surpasses 10 [deg]. Nonlinear responses in pitch angular displacements are identified for *"High Sea States"* since the water plane is not maintained constant due to the geometrical nonlinearities induced by float geometry. The system has proved its capability to return to its equilibrium position for all cases tested, and thus appears to be robust and safe under sea extreme cases. The natural frequency of the system is identified sitting in short-wave periods, where the force exerted by the waves is considerably smaller than for long wave periods, where the design will ride over wave's excitation leading to relatively small loads. In addition, the RAO responses evaluated present similarities when the wave period varies in "*Low*" and "*High*" Sea States. Hence, it is possible to formulate period dependent generalized equations to predict RAO responses for both *Sea States* considered. The mathematical fitting allows the evolution of any set of wave variables within the range of study to be described by adjusting the system damping parameters, in turn obtain calibrated simulation results. This procedure is demonstrated for the case of $H =$ 12 [m], which gives a very good agreement between the model and experiments even allowing for the limited amount of experimental data available for that case. All simulations presented in this paper

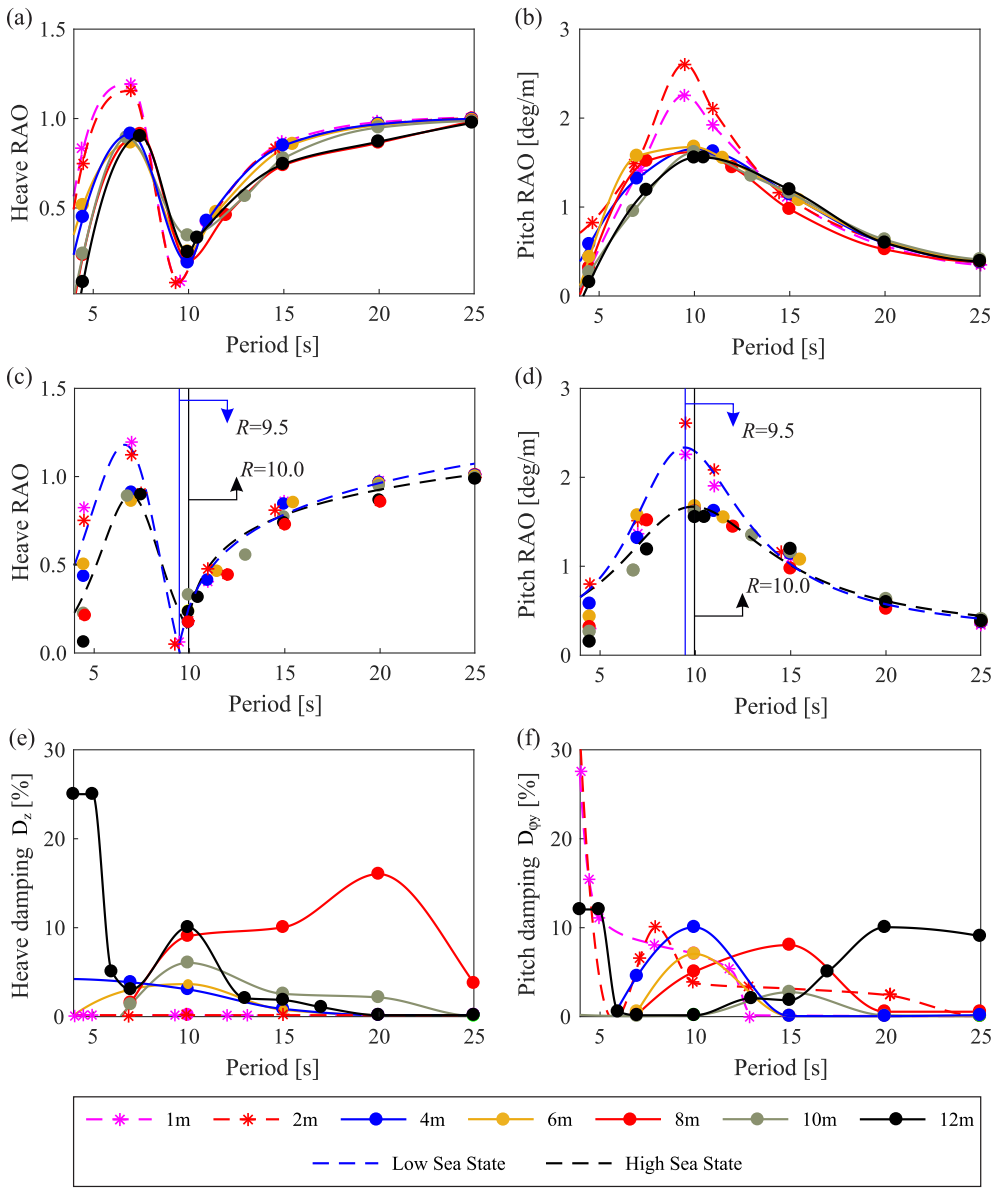

Fig. 10. Matching wave basin experimental results with frequency dependent simulation damping. (a–b) Experimental and simulation heave and pitch RAOs responses for wave periods $T \in [4.5–25]$ [s] and wave heights $H \in [1, 2, 4, 6, 8, 10, 12]$ [m]. (c–d) Generalization of the heave and pitch responses into *"Low Sea States"* for $H = 1$ [m] and $H = 2$ [m] (dashed blue line) and *"High Sea States"* for $H = 4, 6, 8, 10$ and 12 [m] (dashed black line), where R denotes resonant period for each state, respectively. (e–f) Damping ratios as a function of wave period T, that allow to achieve match between experimental and numerical results shown in panels (a–b) (See Fig. A.12).

are validated with experimental tests performed with a scaled 1:60 prototype in a towing tank applying Froude scaling. Model damping coefficients of the sub-structure in contact with the sea environment are adjusted in the marine simulator to achieve a better experimental-simulation agreement and a set of coupled heave and pitch damping coefficients are obtained for each case study. These are expressed with continuity for a range of $T \in [4.5–26]$ [s] utilizing spline interpolation. Moreover, the system heave and pitch displacement time histories are matched with experimental data validating the simulations and system parameter adjustments. The supplementary material of this paper contains a video showing a comparison of responses from the wave tank and the marine simulator, which illustrates agreement between both approaches for wave height of 12 m and wave period of 20 s.

Finally, this work has demonstrated that the virtual prototyping model proposed for the novel FOWT concept designed by T-Omega Wind, and the methodology used by the marine simulator to predict system dynamic responses under periodic wave excitation only requires system damping adjustment to take fully into account the non-linearities in fluid–structure interaction, leading to an excellent experiment-simulation agreement. In addition, it has been identified that most of the ranges of wave parameter values for which the system stability presents an acceptable performance lie within the range of wave heights and periods present in the UK coasts. Therefore, it is a valid indicator of the system's feasibility and will allow further optimization of the design to enlarge the range of system's stability for a specific worldwide location and conditions. Since the model is validated with experimental results, it can be utilized for other purposes such as the study of dynamics and feasibility of towing systems with the marine simulator. The next lines of investigation proposed are the study of the system's performance under other types of wave spectrum excitation (i.e. JONSWAP spectrum) and the study of the floating system dynamics when towed under different wave parameters. The marine simulator can be utilized to study the stability and feasibility for deploying, maintenance and decommissioning operations of FOWT

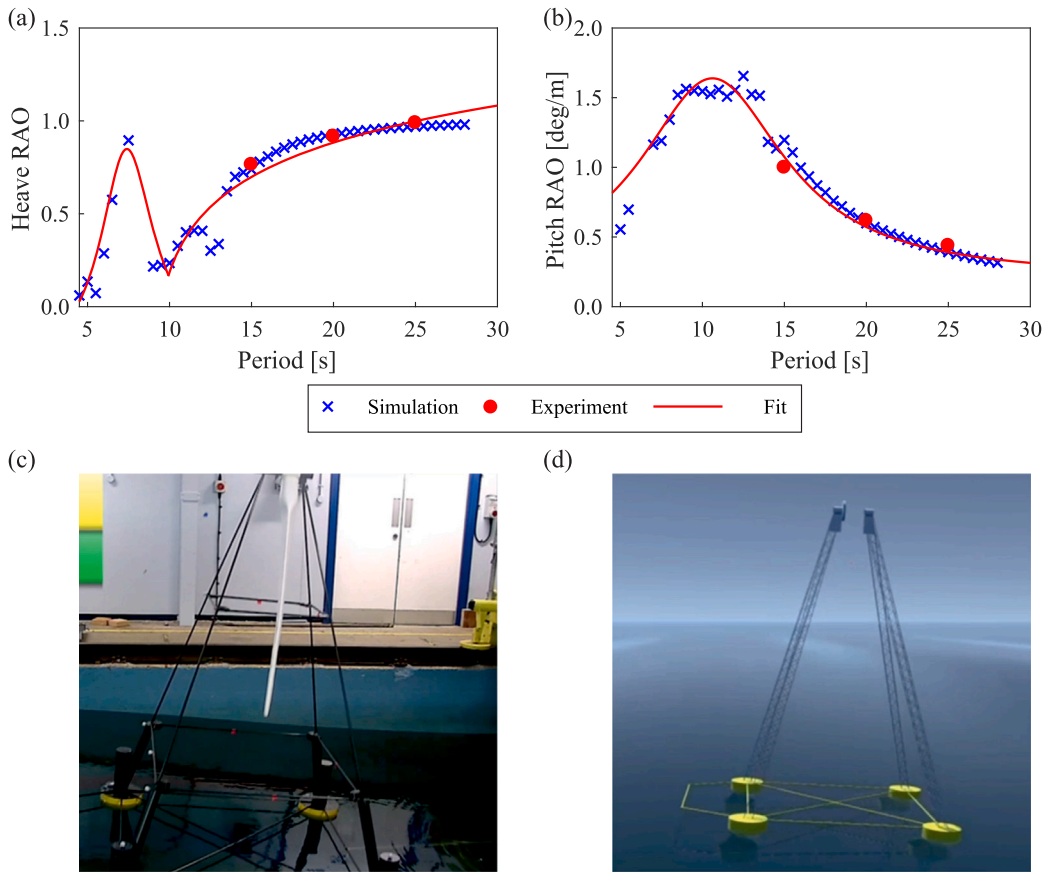

Fig. 11. System dynamic responses with float pitch damping adjustment for *"High Sea States"* approximation and comparison between Simulations (blue colour) and experimental results (red colour) for wave heights of $H = 12$ [m]. (a–b) Heave and pitch RAOs evolution in $T \in [4.5–28]$ [s]. (c–d) Experimental and simulation visual results for $T = 20$ [s].

and the investigation of other parameters that can influence the system dynamics.

CRediT authorship contribution statement

Alicia Terrero-Gonzalez: Formal analysis, Investigation, Methodology, Validation, Writing – original draft. **Saishuai Dai:** Investigation, Resources, Writing – review & editing. **Richard D. Neilson:** Funding acquisition, Writing – review & editing. **Jim Papadopoulos:** Investigation, Resources, Writing – review & editing. **Marcin Kapitaniak:** Writing – review & editing, Visualization, Supervision, Project administration, Funding acquisition, Conceptualization.

Declaration of competing interest

The authors declare the following financial interests/personal relationships which may be considered as potential competing interests: The four university-employed authors declare that they have no known competing financial interests or personal relationships that could have appeared to influence the work reported in this paper. Jim Papadopoulos, co-founder and Chief Engineer of T-Omega Wind, served as a manuscript reviewer/editor and did not otherwise influence the investigation or the presentation of results.

Data availability

Data will be made available on request.

Acknowledgements

The authors wish to thank T-Omega Wind Ltd for their support towards this project and the TechX Accelerator Program for funding the experimental tests performed at the KHL. This work has benefited from the support and funding received from Net Zero Technology Centre and The University of Aberdeen, United Kingdom through their partnership in the National Decommissioning Centre (NDC) and the Scottish Government's Decommissioning Challenge Fund in part-funding the establishment of the marine simulator research facility at the NDC.

Appendix A. *High Sea States* model validation

The damped adjusted model for *High Sea States* is validated with experimental tests performed with the 1:60 prototype in a towing tank for discrete wave parameters of heights ($H = [4,6,8,10,12]$ m) and periods ($T \in [7–25]$ s). The model is validated with the heave and pitch RAO structure displacements showing a similar trend with period evolution and good fit for discrete values; Fig. A.12(a,b) show the comparison between simulation while experimental results for Heave RAO and Fig. A.12(c,d) show the Pitch RAO comparison results validating the model for *High Sea States*.

Appendix B. Heave and pitch fit parameters for *Low Sea States*

Table B.5 present the parameters used to fit heave and pitch RAO responses for wave height of 1 and 2 [m] shown in Section 5 used in Eqs. (15) and (16).

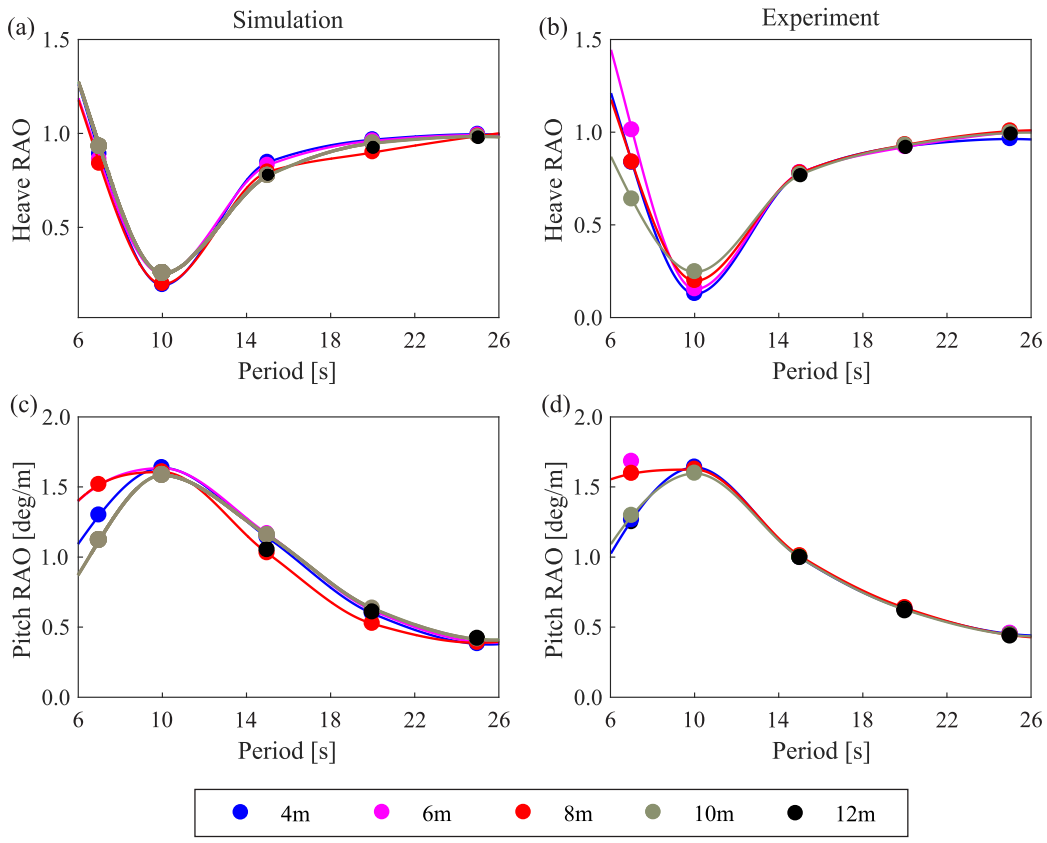

Fig. A.12. *High Sea States* model validation with scaled prototype experimental data for evolution of heave and pitch RAOs for selected wave parameters, where $T \in [6–25]$ [s] and H = [4,6,8,10 and 12] [m]. Point markers show the available experimental and its correspondent simulation value. (a–c) Simulation heave and pitch RAO results for discrete T values and (b–d) Experimental heave and pitch RAO results for discrete T values.

Table B.5
Heave and pitch RAOs equation's fit parameter values for *Low Sea States*.

H = 1 [m]					
Heave RAO fit				Heave RAO fit	
Parameter	Value	Parameter	Value	Parameter	Value
A	9.58	a	9.847	A	24.00
X_o	5.96	d	0.184	X_o	9.87
e	0.000	c	0.462	e	0.128
b	6.76			b	6.2
α	0.81			α	−0.20
R = 9.5					
H = 2 [m]					
Heave RAO fit				Heave RAO fit	
Parameter	Value	Parameter	Value	Parameter	Value
A	8.47	a	9.916	A	24.00
X_o	6.0 0	d	0.167	X_o	10.50
e	0.000	c	0.448	e	0.247
b	8.6			b	8.0
α	0.90			α	−0.60
R = 9.5					

Appendix C. Supplementary data

Supplementary material related to this article can be found online at https://doi.org/10.1016/j.renene.2024.120454.

References

[1] A. Subbulakshmi, M. Verma, M. Keerthana, S. Sasmal, P. Harikrishna, S. Kapuria, Recent advances in experimental and numerical methods for dynamic analysis of floating offshore wind turbines—An integrated review, Renew. Sustain. Energy Rev. 164 (2022) 112525.

[2] E.C. Edwards, A. Holcombe, S. Brown, E. Ransley, M. Hann, D. Greaves, Evolution of floating offshore wind platforms: A review of at-sea devices, Renew. Sustain. Energy Rev. 183 (2023) 113416.

[3] E.C. Edwards, A. Holcombe, S. Brown, E. Ransley, M. Hann, D. Greaves, Trends in floating offshore wind platforms: A review of early-stage devices, Renew. Sustain. Energy Rev. 193 (2024) 114271.

[4] G. Stewart, M. Muskulus, A review and comparison of floating offshore wind turbine model experiments, Energy Procedia 94 (2016) 227–231.

[5] GWEC, Global Wind Report 2023, Global Wind Energy Council, 2023.

[6] T. Stehly, P. Duffy, 2021 Cost of wind Energy Review, National Renewable Energy Laboratory (NREL), 2021.

[7] A. Terrero Gonzalez, P. Dunning, I. Howard, K. McKee, M. Wiercigroch, Is wave energy untapped potential? Int. J. Mech. Sci. 205 (2021) 106544.

[8] J.M. Jonkman, D. Matha, Dynamics of offshore floating wind turbines—analysis of three concepts, Wind Energy 14 (4) (2011) 557–569.

[9] Q. Liu, W. Miao, M. Yue, C. Li, B. Wang, Q. Ding, Dynamic response of offshore wind turbine on 3× 3 barge array floating platform under extreme sea conditions, China Ocean Eng. 35 (2) (2021) 186–200.

[10] K.M. Kopperstad, R. Kumar, K. Shoele, Aerodynamic characterization of barge and spar type floating offshore wind turbines at different sea states, Wind Energy 23 (11) (2020) 2087–2112.

[11] M. Leimeister, Floating offshore wind turbine systems, in: Reliability-Based Optimization of Floating Wind Turbine Support Structures, Springer, 2023, pp. 49–52.

[12] R. Martinez, S. Arnau, C. Scullion, P. Collins, R.D. Neilson, M. Kapitaniak, Variable buoyancy anchor deployment analysis for floating wind applications using a Marine Simulator, Ocean Eng. 285 (2023) 115417.

[13] K. Thiagarajan, H. Dagher, A review of floating platform concepts for offshore wind energy generation, J. Offshore Mech. Arct. Eng. 136 (2) (2014) 020903.

[14] N. Sergiienko, L. da Silva, E. Bachynski-Polić, B. Cazzolato, M. Arjomandi, B. Ding, Review of scaling laws applied to floating offshore wind turbines, Renew. Sustain. Energy Rev. 162 (2022) 112477.

[15] C. Ramachandran, C. Desmond, F. Judge, J.-J. Serraris, J. Murphy, Floating offshore wind turbines: Installation, operation, maintenance and decommissioning challenges and opportunities, Wind Energy Sci. Discuss. 2021 (2021) 15.

[16] H. Tian, M.N. Soltani, M.E. Nielsen, Review of floating wind turbine damping technology, Ocean Eng. 278 (2023) 114365.
[17] J. McMorland, M. Collu, D. McMillan, J. Carroll, Operation and maintenance for floating wind turbines: A review, Renew. Sustain. Energy Rev. 163 (2022) 112499.
[18] Acteon, What needs to be considered when designing the mooring system for a floating wind turbine? URL https://acteon.com/blog/floating-wind-mooring-options/.
[19] T-Omega Wind Ltd., Industrialized multi-benefit floating wind system, 2022, private communication.
[20] OSC, OSC services. URL https://osc.no/.
[21] A. Dynamics, Algoryx dynamics documentation. URL https://www.algoryx.se/documentation/complete/agx/tags/latest/doc/UserManual/source/index.html.
[22] Scottish Government, Scotland's Marine Assessment 2020, Wave Climate, Marine Scotland Assessment, 2020.
[23] OSC, FATHOM HYDRO, User Manual, Version 0.6, Tech. rep., Offshore Simulator Centre, 2022.
[24] Orcina, Orcaflex, Vessel theory: Wave drift and sum frequency loads. URL https://www.orcina.com/webhelp/OrcaFlex/Content/html/Vesseltheory, Wavedriftandsumfrequencyloads.htm.
[25] L. Zhang, W. Shi, M. Karimirad, C. Michailides, Z. Jiang, Second-order hydrodynamic effects on the response of three semisubmersible floating offshore wind turbines, Ocean Eng. 207 (2020) 107371.
[26] J. Pinkster, Low-frequency phenomena associated with vessels moored at sea, Soc. Pet. Eng. J. 15 (06) (1975) 487–494.
[27] J. Newman, Second order, slowly-varying forces on vessels in irregular waves, in: Intl. Symp. Dyn. Marine Vehicle & Struc Waves, Mech. Engng. Pub., London (UK), 1974.
[28] L.H. Carmo, A.N. Simos, On the complementarity of the slender-body and Newman's approximations for difference-frequency second-order wave loads on slender cylinders, Ocean Eng. 259 (2022) 111905.
[29] L. Wang, J. Jonkman, J. Papadopoulos, A.T. Myers, OPENFAST Modeling of the T-Omega Wind floating offshore wind turbine system, in: 5th International Offshore Wind Technical Conference, IOWTC, 2023, 119410.
[30] J. Chen, Z. Liu, Y. Song, Y. Peng, J. Li, Experimental study on dynamic responses of a spar-type floating offshore wind turbine, Renew. Energy 196 (2022) 560–578.
[31] S. Cao, Y. Cheng, J. Duan, X. Fan, Experimental investigation on the dynamic response of an innovative semi-submersible floating wind turbine with aquaculture cages, Renew. Energy 200 (2022) 1393–1415.
[32] D. Skandali, E. Lourens, R. Ogink, Calibration of response amplitude operators based on measurements of vessel motions and directional wave spectra, Mar. Struct. 72 (2020) 102774.
[33] P. Aboutalebi, F. M'zoughi, I. Martija, I. Garrido, A.J. Garrido, Switching control strategy for oscillating water columns based on response amplitude operators for floating offshore wind turbines stabilization, Appl. Sci. 11 (11) (2021) 5249.
[34] S.K. Das, M. Baghfalaki, Mathematical modelling of response amplitude operator for roll motion of a floating body: Analysis in frequency domain with numerical validation, J. Mar. Sci. Appl. 13 (2014) 143–157.
[35] G. Ramachandran, A. Robertson, J. Jonkman, M.D. Masciola, Investigation of response amplitude operators for floating offshore wind turbines, in: ISOPE International Ocean and Polar Engineering Conference, ISOPE, 2013, pp. ISOPE–I.
[36] M. Yue, Q. Liu, C. Li, Q. Ding, S. Cheng, H. Zhu, Effects of heave plate on dynamic response of floating wind turbine Spar platform under the coupling effect of wind and wave, Ocean Eng. 201 (2020) 107103.
[37] H. Lee, D.-J. Lee, Effects of platform motions on aerodynamic performance and unsteady wake evolution of a floating offshore wind turbine, Renew. Energy 143 (2019) 9–23.
[38] S. Fu, Z. Li, W. Zhu, X. Han, X. Liang, H. Yang, W. Shen, Study on aerodynamic performance and wake characteristics of a floating offshore wind turbine under pitch motion, Renew. Energy 205 (2023) 317–325.
[39] A.L. Stancik, E.B. Brauns, A simple asymmetric lineshape for fitting infrared absorption spectra, Vib. Spectrosc. 47 (1) (2008) 66–69.